IEEE Access
Multidisciplinary | Rapid Review | Open Access Journal

Received 16 May 2022, accepted 22 June 2022, date of publication 30 June 2022, date of current version 8 July 2022.

Digital Object Identifier 10.1109/ACCESS.2022.3187403

RESEARCH ARTICLE

Evaluation of Numerical Methods for TSCOPF in a Large Interconnected System

MOHAMMADAMIN AGHAHASSANI, EDGARDO D. CASTRONUOVO, (Senior Member, IEEE), PABLO LEDESMA, AND FRANCISCO ARREDONDO

Department of Electrical Engineering, Universidad Carlos III de Madrid, 28911 Leganés, Spain

Corresponding author: Mohammadamin Aghahassani (maghahas@ing.uc3m.es)

This work was supported by the Spanish Agencia Estatal de Investigación under Project PID2019-104449RB-I00 and Project AEI/10.13039/501100011033.

ABSTRACT Transient stability-constrained optimal power flow (TSCOPF) models comprehensively analyze the security and economic operation of power systems. However, they require a high computational effort and can suffer from convergence problems when applied to large systems. This study analyzes the performance of eleven numerical integration algorithms applied to ordinary differential equations that represent power system dynamics in a TSCOPF model. The analyzed algorithms cover a range of explicit and implicit methods, including the recently published semi-explicit and semi-implicit Adams-Bashforth-Moulton formulas, together with several initialization techniques. The integration methods are applied to a model of the Iberian Peninsula power system, and their performance is discussed in terms of convergence, accuracy, and computational effort. The results show that most implicit methods converge to the solution, even for large time steps. In particular, the Adams-Moulton method of order two and Simpson's rule, both initialized with RK4, outperform the trapezoidal rule, which is the default method in TSCOPF models.

INDEX TERMS Numerical methods, optimal power flow, power system stability, transient stability, TSCOPF.

NOMENCLATURE

z	Generation cost (in $\frac{€}{h}$).
N_g, N_b	Number of synchronous generators and buses, respectively.
c_i	Cost coefficient of the synchronous generator at bus i (in $\frac{€}{MWh}$).
$P_{g,i,0}$, $Q_{g,i,0}$	Steady-state active and reactive power generated by the synchronous generator at bus i (in p.u.).
$P_{g,i,t}$, $Q_{g,i,t}$	Active and reactive power generated by the synchronous generator at bus i and time t (in p.u.).
$P_{d,i,t}$, $Q_{d,i,t}$	Active and reactive load at bus i and time t (in p.u.).
$P_{e,i,t}$, $Q_{e,i,t}$	Electric output active and reactive power in the rotor of the synchronous generator at bus i and time t (in p.u.).
$P_{m,i}$	Mechanical input power of the synchronous generator at bus i (in p.u.).
$V_{i,0}$, $\alpha_{i,0}$	Steady state voltage magnitude and angle at bus i (in p.u. and rad, respectively).
$V_{i,t}$, $\alpha_{i,t}$	Voltage magnitude and angle at bus i and time t (in p.u. and rad, respectively).
I_{br}	Steady state current of branch br (in p.u.).
$Y_{i,j}$, $\theta_{i,j}$	Magnitude and angle of the element (i,j) in the bus admittance matrix Y (in p.u. and rad, respectively).
$Y_{L,br,j}$, $\theta_{L,br,j}$	Magnitude and angle of the element (br,j) in the line admittance matrix Y_L (in p.u. and rad, respectively).
$\delta_{i,t}$	Rotor angle of synchronous generator i at time t in synchronously rotating reference frame (in rad).

The associate editor coordinating the review of this manuscript and approving it for publication was Siqi Bu.

$\delta_{COI,t}$	The rotor angle corresponds to the center of inertia (COI) at time t (in rad).
ω_s	Synchronous rotor speed (in $\frac{rad}{s}$).
$\Delta\omega_{i,0}$	Steady-state rotor speed deviation of the synchronous generator at bus i (in p.u.).
$\Delta\omega_{i,t}$	Rotor speed deviation of the synchronous generator at bus i and time t (in p.u.).
$x'_{d,i}$	Direct axis transient reactance of the synchronous generator at bus i (in p.u.).
$E'_{I,i}$	Internal voltage of the synchronous generator at bus i (in p.u.).
H_i	Inertia constant of the synchronous generator at bus i (in s).
D_i	Damping factor of the synchronous generator at bus i (in p.u.).
V^{min}, V^{max}	Lower and upper limits of the bus voltage magnitude (in p.u.).
I_{br}^{max}	Limit of the current in branch br (in p.u.).
$P_{g,i}^{max}$	Limit of the active power generated by the synchronous generator at bus i (in p.u.).
$Q_{g,i}^{min}$, $Q_{g,i}^{min}$	Lower and upper limits of the reactive power generated by the synchronous generator at bus i (in p.u.).
δ^{max}	Limit of the rotor angle (in rad).
Δt	Integration time step (in s).

I. INTRODUCTION

Transient stability-constrained optimal power flow (TSCOPF) is an optimization problem that offers a comprehensive approach to power system optimization by simultaneously addressing economic and operational objectives while considering both static and dynamic stability constraints. TSCOPF has recently received increasing attention [1], [2] because system operators are forced to operate power systems close to their operational limits owing to the high penetration of non-programmable renewable generation, liberalized electricity markets, and environmental restrictions.

The size and complexity of interconnected power systems make large-scale TSCOPF problems challenging, with several authors following different approaches [3], [4]. One approach, followed in [5], formulates TSCOPF as a nonlinear programming problem (NLP) in which, the dynamic behavior of the power system is obtained using PSS/E, an external power system simulator independent of the optimization problem. In this sequential technique, the generation dispatch changes at each iteration based on simulation results and constraint violations. This method has the problem of falling into numerical instabilities and convergence problems when simulating transiently unstable cases.

A more common approach followed in this work is to use a simultaneous discretization algorithm [6] that directly incorporates the dynamic simulation in the optimization problem. In [2], [7]–[13], differential equations describing power system dynamics are transformed into corresponding algebraic equations using a numerical integration algorithm. They are then added to the power flow equations. The resulting optimization problem is then solved using an NLP solver. This technique is robust and can handle unstable cases; however, it becomes computationally demanding when applied to large power systems.

A. LITERATURE REVIEW

Although there are different families of numerical methods for integrating differential equations [14]–[22], the trapezoidal rule is practically the only method used in TSCOPF studies based on simultaneous discretization [2], [8], [9], [11], [14], [23], [24], because it is easy to program and numerically stable. To the knowledge of the authors, there are no previous studies on the performance of numerical methods in TSCOPF models, except for [7] and [25], which investigated a limited number of methods in a relatively small system. This study explores a broader range of integration methods to reduce the computation time in large-scale TSCOPF models.

Numerical methods can be classified as explicit or implicit. The explicit algorithms use known quantities from past steps to directly obtain the solution to the current step, whereas the implicit methods require current and prior steps for the calculation. Most commercial power system simulators use explicit numerical methods because they are easier to implement. PowerWorld, for instance, uses second-order Runge-Kutta [26], whereas PSS/E and PSLF use second-order Adams-Bashforth [27]. The implicit methods are numerically more stable and better suited to stiff systems than the explicit methods, but this comes at the cost of solving nonlinear equations at each step, resulting in higher computational time. In general, there should be a trade-off between numerical stability and computational cost. Predictor-corrector methods combine some advantages of implicit and explicit methods. A predictor-corrector method uses two sets of equations, one for prediction and the other for correction. In [21] and [22], the conventional predictor-corrector Adams-Bashforth-Moulton (ABM) method is modified to construct semi-explicit and semi-implicit ABMs, improving the computation accuracy.

Numerical methods can also be classified based on the number of steps required for each iteration. Single-step methods are based solely on the previous step; for example, the Runge-Kutta fourth-order (RK4) method has an accuracy of order four but at the cost of significant computation time because four function evaluations are required at each time step [28], [29]. As the computation time is a critical issue in TSCOPF models, it is preferable to use multistep methods that require only one function evaluation at each step and improve the accuracy by using data from several previous steps. The number of steps in this study is limited to two because, while increasing the number of steps improves accuracy, it also threatens numerical stability [30].

Moreover, two-step methods require two successive starting points for the initialization. The initial condition provides

the first starting point, and the second starting point can be calculated using another one-step method, such as Euler, trapezoidal rule, or RK4. Therefore, it is important to consider the error incurred when approximating this extra initial point because it may affect the final solution.

B. CONTRIBUTION

The main contribution of this work is a comprehensive analysis of numerical methods in an optimization model based on simultaneous discretization. The model is solved using a standard interior-point algorithm, which is the main approach in TSCOPF. The results show that alternative methods can outperform the trapezoidal rule in TSCOPF applications. The performance of each method is tested on a 216-buses, 75-generators model of the Iberian Peninsula system, including Portugal and Spain, in which six severe contingencies are evaluated. These methods are discussed in terms of accuracy, computational time, and numerical stability. Additionally, the effect of initialization on the accuracy of two-step methods is analyzed. The result is a set of suitable methods that can serve as better alternatives to the trapezoidal rule in future TSCOPF studies.

The remainder of this paper is organized as follows. Section II develops the optimization model. Section III describes several numerical methods applied to the TSCOPF model. Section IV introduces a case study. Section V presents simulation results. Finally, conclusions are presented in Section VI.

II. OPTIMIZATION MODEL

The optimization problem consists of an objective function minimizing the generation cost (1) and a set of nonlinear equality and inequality constraints (2)-(16):

$$z = min \sum_{i=1}^{N_g} c_i P_{g,i,0} \tag{1}$$

subjected to

$$P_{g,i,t} - P_{d,i,t} = V_{i,t} \sum_{j=1}^{N_b} V_{j,t} Y_{i,j} cos(\alpha_{i,t} - \alpha_{j,t} - \theta_{i,j}) \tag{2}$$

$$Q_{g,i,t} - Q_{d,i,t} = V_{i,t} \sum_{j=1}^{N_b} V_{j,t} Y_{i,j} sin(\alpha_{i,t} - \alpha_{j,t} - \theta_{i,j}) \tag{3}$$

$$P_{e,i,t} x'_{d,i} = E'_{I,i} V_{i,t} sin(\delta_{i,t} - \alpha_{i,t}) \tag{4}$$

$$Q_{e,i,t} x'_{d,i} = (E'_{I,i})^2 - E'_{I,i} V_{i,t} cos(\delta_{i,t} - \alpha_{i,t}) \tag{5}$$

$$P_{a,i,t} = P_{m,i} - P_{e,i,t} \tag{6}$$

$$\frac{d\delta_{i,t}}{dt} = \omega_s \Delta\omega_{i,t} \tag{7}$$

$$\frac{d\Delta\omega_{i,t}}{dt} = \frac{1}{2H_i}(P_{a,i,t} - D_i \Delta\omega_{i,t}) \tag{8}$$

$$\Delta\omega_{i,0} = 0 \tag{9}$$

$$\delta_{COI,t} = \sum_{i=1}^{N_b} \frac{H_i \delta_{i,t}}{H_i} \tag{10}$$

$$I_{br} = \sum_{j=1}^{N_b} Y_{L,br,j} V_{j,0} [cos(\theta_{L,br,j} + \alpha_{j,0}) + jsin(\theta_{L,br,j} + \alpha_{j,0})] \tag{11}$$

$$V^{min} \le V_{i,0} \le V^{max} \tag{12}$$

$$|I_{br}| \le I_{br}^{max} \tag{13}$$

$$0 \le P_{g,i,0} \le P_{g,i}^{max} \tag{14}$$

$$Q_{g,i}^{min} \le Q_{g,i,0} \le Q_{g,i}^{max} \tag{15}$$

$$-\delta^{max} \le \delta_{i,t} - \delta_{COI,t} \le \delta^{max} \tag{16}$$

Table 1 summarizes the physical meaning of each equation. Wind power plants are modeled as a fixed generation with a power factor of one and a cost of zero. The transient stability limit (16) is determined as the maximum rotor angle deviation from the center of inertia (COI), as is customary in TSCOPF studies [11], [13]. Equations (1)-(16) represent a typical TSCOPF model based on simultaneous discretization that provides the optimal dispatch with steady-state and transient stability limits after a severe fault. When the solution provided by the OPF becomes unstable, the stability limit imposed by (16) modifies the OPF generation dispatch, thereby increasing the cost of obtaining a secure operation.

In the TSCOPF model, differential equations (7) and (8) are discretized using a numerical algorithm and solved simultaneously with (1)-(6) and (9)-(16) using an NLP solver. However, in conventional transient stability simulations, (7) and (8) are discretized and solved sequentially. TSCOPF provides an optimal dispatch together with the simulation of the fault included in the model; this simulation coincides with a conventional transient stability simulation that takes the optimal dispatch as the initial point.

Fig. 1 shows the procedure used to build and solve the TSCOPF model. A Python program reads all relevant data, builds the pre-fault, fault, and post-fault admittance matrices for each contingency, and writes the TSCOPF model containing (1)-(16) in the GAMS modeling language. In this work, at the block marked with an arrow in Fig. 1, different numerical integration methods are used to discretize differential equations (7) and (8). For example, applying the trapezoidal rule, which is the default method in TSCOPF, to (7) and (8) yields:

$$\delta_{i,n} - \delta_{i,n-1} = \frac{\omega_s \Delta t}{2}(\Delta\omega_{i,n} + \Delta\omega_{i,n-1}), \tag{17}$$

$$\left(1 + \frac{D_i \Delta t}{4H_i}\right) \Delta\omega_{i,n} - \left(1 - \frac{D_i \Delta t}{4H_i}\right) \Delta\omega_{i,n-1} = \frac{\Delta t}{4H}(P_{a,i,n} + P_{a,i,n-1}). \tag{18}$$

The complete TSCOPF model is then solved in GAMS using the interior-point optimizer IPOPT, which is an NLP solver suited for large-scale nonlinear optimization problems. The model is managed directly by IPOPT, and there is no need for a power system solver outside the GAMS solver.

TABLE 1. Optimization model constraints.

Equality constraints	AC power flow equations (2)-(3)
	Synchronous generator algebraic equations (4)-(6)
	Synchronous generator differential equations (7)-(8)
	Initial conditions (9)
	COI calculation (10)
	Transmission lines current (11)
Inequality constraints	Steady-state limits[a] (12)-(15)
	Transient stability limit[b] (16)

[a] bus voltage limits, line current limits, generation limits.
[b] rotor angle deviation limit w.r.t the COI.

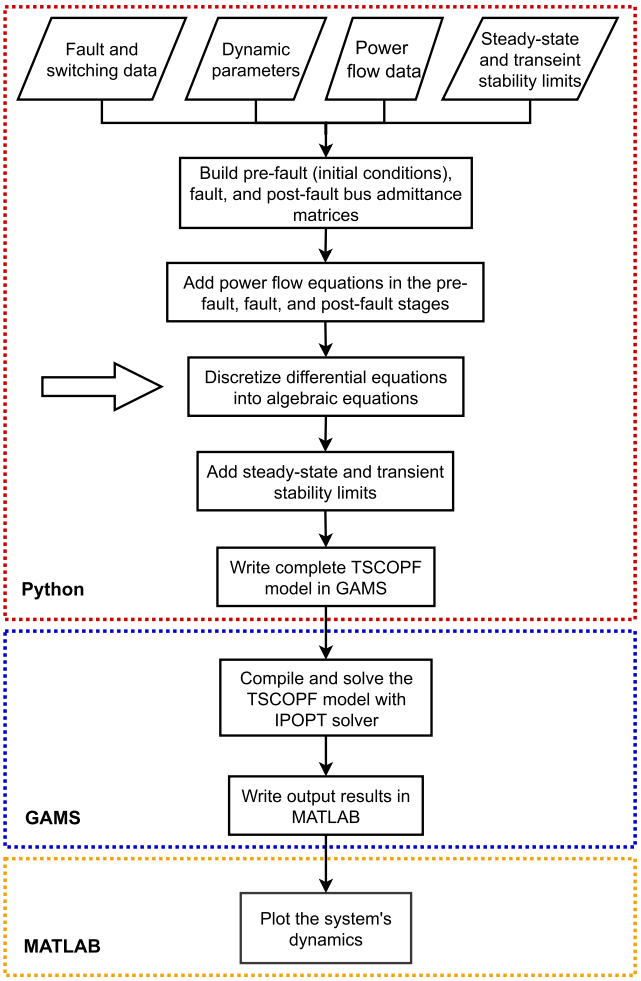

FIGURE 1. Flowchart showing the implementation of the TSCOPF model.

III. NUMERICAL METHODS

A set of representative numerical methods for the solution of ordinary differential equations (ODEs) (7) and (8) is selected to evaluate their performance in the TSCOPF model. These methods correspond to some of the most commonly used two-step algorithms [31] and newly constructed semi-explicit and semi-implicit methods. The ODEs representing the power system dynamics can be expressed as:

$$\frac{d\mathbf{x}}{dt} = \mathbf{f}(\mathbf{x}, t) \quad \text{with} \quad \mathbf{x}(t_0) = \mathbf{x_0}, \tag{19}$$

where $\mathbf{x}$ is the vector of state variables, $\mathbf{x_0}$ is the vector of initial conditions at $t = t_0$, and $\mathbf{f}(\mathbf{x}, t)$ is a known function.

A. TWO-STEP METHODS

Most numerical methods described in this section can be defined using the following generic expression:

$$\alpha_0\mathbf{x_n} + \alpha_1\mathbf{x_{n-1}} + \alpha_2\mathbf{x_{n-2}} = \Delta t(\beta_0\mathbf{f_n} + \beta_1\mathbf{f_{n-1}} + \beta_2\mathbf{f_{n-2}}), \tag{20}$$

where $\mathbf{x_n}$ is the vector of numerical approximations of exact solutions $\mathbf{x}(t_n)$ at time $t_n = t_0 + n\Delta t$; α_i and β_i are the coefficients representing different numerical methods; and $\mathbf{f_n} = \mathbf{f}(\mathbf{x(t_n)}, t_n)$. The application of (20) to (7) and (8) results in:

$$\alpha_0\delta_{i,n} + \alpha_1\delta_{i,n-1} + \alpha_2\delta_{i,n-2} = \Delta t\omega_s(\beta_0\Delta\omega_{i,n} + \beta_1\Delta\omega_{i,n-1} + \beta_2\Delta\omega_{i,n-2}), \tag{21}$$

and

$$\begin{aligned}\alpha_0\Delta\omega_{i,n} + \alpha_1\Delta\omega_{i,n-1} + \alpha_2\Delta\omega_{i,n-2} &= \frac{\Delta t}{2H_i}[\beta_0(P_{a,i,n} - D_i\Delta\omega_{i,n}) \\ &\quad + \beta_1(P_{a,i,n-1} - D_i\Delta\omega_{i,n-1}) \\ &\quad + \beta_2(P_{a,i,n-2} - D_i\Delta\omega_{i,n-2})].\end{aligned} \tag{22}$$

Table 2 lists the names and main characteristics of some of the analyzed methods. A discussion about the accuracy and numerical stability of these methods can be found in [31]. One method does not have a unique name and is thus referred to as method A. The specific equation of each method in the TSCOPF model can be found by substituting parameters α_i and β_i in (21) and (22). For example, the Adams-Moulton method of order two can be formulated as:

$$\delta_{i,n} - \delta_{i,n-1} = \omega_s\Delta t\left(\frac{5}{12}\Delta\omega_{i,n} + \frac{8}{12}\Delta\omega_{i,n-1} - \frac{1}{12}\Delta\omega_{i,n-2}\right), \tag{23}$$

and

$$\begin{aligned}\Delta\omega_{i,n} - \Delta\omega_{i,n-1} = \frac{\Delta t}{2H_i}\Bigg(&\frac{5}{12}(P_{a,i,n} - D_i\Delta\omega_{i,n}) \\ &+\frac{8}{12}(P_{a,i,n-1} - D_i\Delta\omega_{i,n-1}) \\ &-\frac{1}{12}(P_{a,i,n-2} - D_i\Delta\omega_{i,n-2})\Bigg).\end{aligned} \tag{24}$$

The trapezoidal rule is the only one-step method in Table 2; the rest are two-step algorithms. One-step numerical methods (if $\alpha_2 = \beta_2 = 0$ in (20)) approximate $\mathbf{x_n}$ using $\mathbf{x_{n-1}}$, the value obtained in the previous step. The starting point $\mathbf{x_0}$ is calculated from initial conditions, typically solving a power flow. Two-step methods, on the other hand, require $\mathbf{x_{n-1}}$ and

TABLE 2. Investigated numerical methods [31].

Method	α_0	α_1	α_2	β_0	β_1	β_2	Type	Step	Order	Error constant	Absolute stability
Adams-Bashforth, AB(2)	1	-1	0	0	3/2	-1/2	explicit	2	2	$5/12$	not A-stable & zero stable
midpoint rule	1	0	-1	0	2	0	explicit	2	2	$1/6$	not A-stable
Trapezoidal rule, TR	1	-1	0	1/2	1/2	0	implicit	1	2	$-1/12$	A-stable & zero-stable
Simpson's rule	1	0	-1	1/3	4/3	1/3	implicit	2	4	$-1/180$	not A-stable & zero stable
Adams-Moulton, AM(2)	1	-1	0	5/12	8/12	-1/12	implicit	2	3	$-1/24$	not A-stable & zero stable
BDF(2)	1	-4/3	1/3	2/3	0	0	implicit	2	2	$-1/3$	A-stable & zero-stable
method A	1	-1	0	3/4	0	1/4	implicit	2	2	n.a.	A_0-stable & zero-stable

$\mathbf{x_{n-2}}$ in the previous two steps. Although the value of $\mathbf{x_0}$ for the initial step is calculated from initial conditions, finding the value of $\mathbf{x_1}$ in a two-step method requires another one-step method such as Euler, trapezoidal rule or RK4.

Two of the methods in Table 2 are explicit, which means that $\beta_0 = 0$ and $\mathbf{x_n}$ can be found explicitly from previous time steps. Explicit two-step methods are not absolutely stable (A-stable); however, Adams-Bashforh is a zero-stable explicit method with the maximum possible order [31]. The rest of the methods in Table 2 are implicit methods, which means that $\mathbf{x_n}$ cannot be directly expressed in terms of known quantities from the previous steps because $\beta_0 \neq 0$.

The methods with the same order of accuracy can produce different levels of error, depending on the error constant. Adams-Moulton with order three gets closer to the exact solution than Adams-Bashforth with order two but at the cost of solving a nonlinear equation at each step. However, the Adams-Moulton is not the highest-order possible implicit method with zero-stability. Simpson's rule with order four reaches the highest order because of its symmetrical structure.

Finally, the trapezoidal rule has the highest possible order among A-stable implicit methods, with the lowest error constant. Since the absolute stability is difficult to obtain, the condition can be lowered to A_0-stability [31].

B. PREDICTOR-CORRECTOR METHODS

Predictor-corrector methods proceed in two stages. The first stage typically uses an explicit method to extrapolate the value at the next point, and the second stage uses an implicit method to refine the initial approximation.

Three predictor-corrector methods are tested in this work: the Adams-Bashforth-Moulton (ABM) method and its two variants, the semi-implicit and semi-explicit Adams-Bashforth-Moulton methods (SIABM and SEABM, respectively). The ABM method applied to (7) and (8) yields:

$$\delta^p_{i,n} - \delta_{i,n-1} = \omega_s \Delta t \left(\frac{3}{2}\Delta\omega_{i,n-1} - \frac{1}{2}\Delta\omega_{i,n-2} \right),$$

$$\Delta\omega^p_{i,n} - \Delta\omega_{i,n-1} = \frac{\Delta t}{2H_i}\left(\frac{3}{2}(P_{a,i,n-1} - D_i\Delta\omega_{i,n-1}) - \frac{1}{2}(P_{a,i,n-2} - D_i\Delta\omega_{i,n-2}) \right),$$

$$\delta_{i,n} - \delta_{i,n-1} = \omega_s \Delta t \left(\frac{5}{12}\Delta\omega^p_{i,n} + \frac{8}{12}\Delta\omega_{i,n-1} - \frac{1}{12}\Delta\omega_{i,n-2} \right),$$

$$\Delta\omega_{i,n} - \Delta\omega_{i,n-1} = \frac{\Delta t}{2H_i}\left(\frac{5}{12}(P^p_{a,i,n} - D_i\Delta\omega^p_{i,n}) + \frac{8}{12}(P_{a,i,n-1} - D_i\Delta\omega_{i,n-1}) - \frac{1}{12}(P_{a,i,n-2} - D_i\Delta\omega_{i,n-2}) \right) \quad (25)$$

The SEABM method modifies the last equation by substituting $P^p_{a,i,n}$ with $P_{a,i,n}$, and the SIABM method additionally substitutes $\Delta\omega^p_{i,n}$ with $\Delta\omega_{i,n}$. A discussion on the numerical properties of ABM, SEABM, and SIABM can be found in [22] and [32].

C. MERGED TRAPEZOIDAL RULE

In addition to the methods listed in Table 2 and the predictor-corrector methods, a method called the merged trapezoidal rule (MTR), is analyzed. The MTR is obtained by merging (17) and (18) and eliminating the speed, which yields:

$$(1 + \frac{D_i\Delta t}{4H_i})\delta_{i,n} - 2\delta_{i,n-1} + (1 - \frac{D_i\Delta t}{4H_i})\delta_{i,n-2} = \frac{\omega_s\Delta t^2}{8H_i}(P_{a,i,n} + 2P_{a,i,n-1} + P_{a,i,n-2}). \quad (26)$$

where the rotor angle deviation $\delta_{i,n}$ is expressed as a function of the two previous steps. As Δt is squared, MTR does not follow the general form of the two-step methods expressed by (20).

IV. CASE STUDY

The numerical methods in Table 2, along with ABM, SEABM, SIABM, and MTR, are implemented in the TSCOPF model described in Section II and applied to a case representing the Iberian Peninsula transmission system. The case is based on the Bialek European model [33], which can be downloaded from the link provided in [34].

Fig. 2 shows the single-line diagram of the studied system, which includes Spain and Portugal and contains 216 buses, 368 transmission lines, 75 generating units, and 143 loads consuming 50.2 GW. The power systems of the rest of continental Europe and Morocco are each reduced to a single equivalent bus connected to a synchronous generator/load. In this study, the Iberian Peninsula exports 700 MW to France and 497 MW to Morocco before the fault. The voltage limits in (12) are set at a minimum of 0.9 p.u. and a maximum of

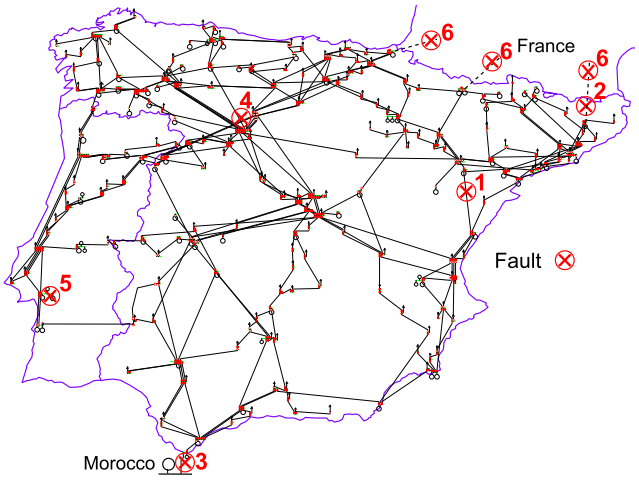

FIGURE 2. Single-line diagram of the Iberian Peninsula transmission system model.

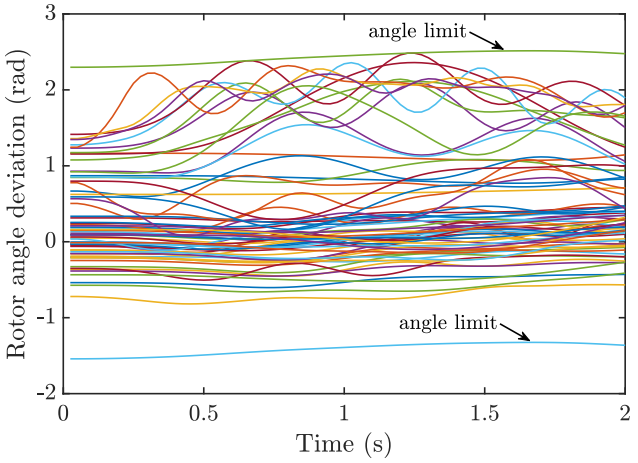

FIGURE 3. Synchronous generator rotor angles. Fault 1.

1.05 p.u. The maximum rotor angle deviation with respect to the COI in (16) is 110°. The complete data, including the parameters of the power system and the static and dynamic constraints, can be found as supplementary material to this document.

The original case was modified to accommodate a total capacity of 9380 MW of wind power. Before the fault, the wind power production was 2345 MW, which amounts to 25 % of the total wind capacity and 5.07 % of the total generation. It has also been modified to account for the reactive power consumption in the loads. Shunt capacitors were added to stabilize the voltages and reduce the reactive power flow in the lines. Six different faults are analyzed. The first four faults are modeled as a short-circuit in a transmission line near a substation and cleared after 200 ms by disconnecting the affected line. Short-circuits are the most challenging faults to analyze in transient stability studies. However, other types of faults, such as a generator outage and the separation of the Iberian Peninsula from the rest of continental Europe, are also explored in this study. The fault locations are marked in Fig. 2. Each fault represents a relevant incident on the power system of the Iberian Peninsula.

- Fault 1 is near a large nuclear power plant (2000 MW) operating at full load.
- Fault 2 is close to one of the tie-lines connecting the Iberian Peninsula to the rest of continental Europe.
- Fault 3 is next to the tie-line connecting the Iberian Peninsula and Morocco.
- Fault 4 is close to a critical substation called La Mudarra, which connects several lines carrying power from power plants to the northwest to loads in the center, where the capital city Madrid is located.
- Fault 5 is the loss of the largest operating power plant (2580 MW) in Portugal.
- Fault 6 is the trip of the three tie-lines connecting the Iberian Peninsula to the rest of continental Europe.

The model is written in GAMS [35] and solved using the IPOPT solver [36]–[38] on a 64-bit personal computer with a 3.60 GHz processor and 24.0 GB RAM. The resulting nonlinear optimization model contains 141,868 variables and 167,181 equality and inequality constraints using the trapezoidal rule and a 10 ms time step.

V. RESULTS

This section compares the performance of the seven methods listed in Table 2, ABM, SEABM, SIABM, and MTR, when applied to differential equations (7) and (8) in the TSCOPF model. The trapezoidal rule, which is the numerical method used by default in TSCOPF based on simultaneous discretization, is highlighted in black in the figures to serve as a term of comparison. The results for Fault 1 in Fig. 2 are discussed in detail in Subsections V-A to V-C. The remaining faults are summarized in Subsection V-D.

Fig. 3 shows an example of the solution of the TSCOPF model in the case of Fault 1. The dispatch provided by TSCOPF ensures transient stability by restricting the angle deviation of each synchronous generator with respect to the COI. Therefore, the total generation cost of the dispatch provided by TSCOPF is higher than the cost obtained with an OPF and this difference can be seen as the cost of ensuring transient stability.

Fig. 4 shows the increase in the TSCOPF total production cost when different numerical methods and time steps are applied to the optimization model. Unless otherwise specified, the trapezoidal rule is used to initialize two-step methods. The solutions tend to converge at approximately 2.4% as the time step decreases. Most of the results are reliable with a time step of 10 ms, which is a common value in transient stability studies.

On the other hand, as the time step increases, the transient stability cost decreases, indicating that the solution is not only less accurate but also less secure. This is because some economic power plants that are more prone to causing a loss of synchronism tend to increase their production. As a result, large time steps might result in operating points that can be transiently unstable during real operations.

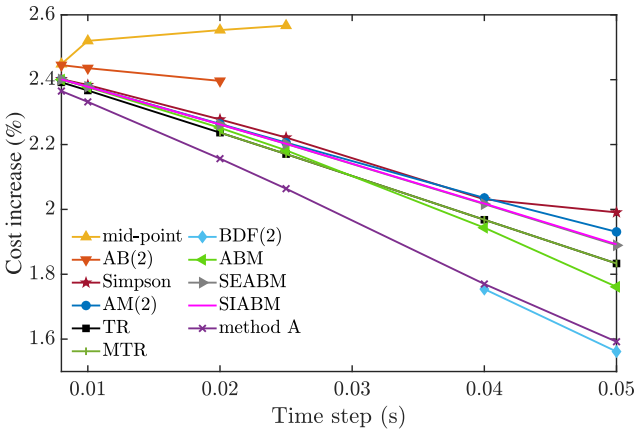

FIGURE 4. Increase in the TSCOPF generation cost compared to the OPF. Fault 1.

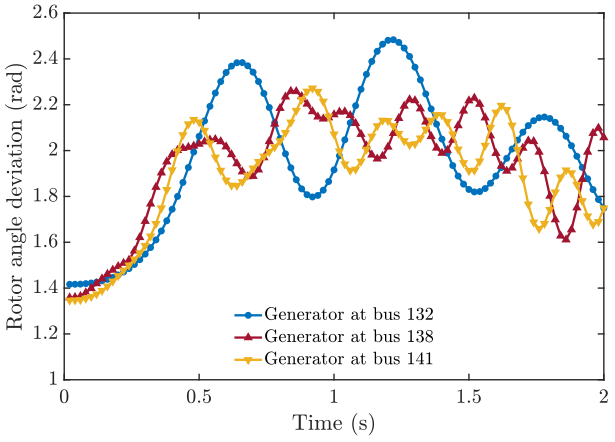

FIGURE 5. Rotor angles of three synchronous generators near the faulted bus. Fault 1, using method AB(2) with time step 20 ms.

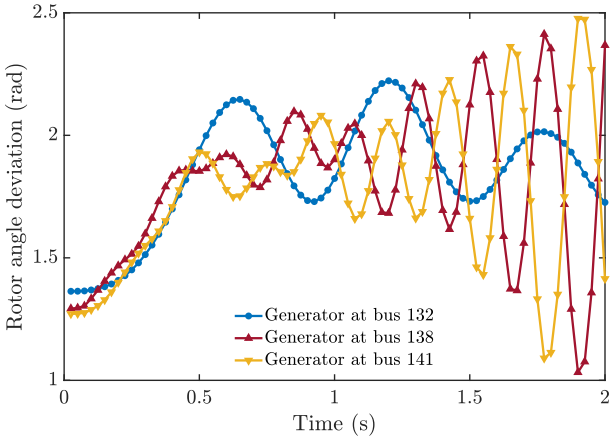

FIGURE 6. Rotor angles of three synchronous generators near the faulted bus. Fault 1, using method AB(2) with time step 25 ms.

A. TWO-STEP IMPLICIT METHODS

Fig. 4 shows that TSCOPF with the BDF(2) method fails to converge for small time steps.

The trapezoidal rule, Simpson's rule, AM(2), ABM, SEABM, SIABM, and, to a lesser extent, method A produce good results in terms of accuracy and convergence, and are deemed suitable for TSCOPF studies. MTR, introduced in Section III-C, provides similar results to the trapezoidal rule for 20 ms and larger time steps, but it does not converge for smaller time steps.

B. TWO-STEP EXPLICIT METHODS

The relatively poor properties of the explicit methods compared with the implicit ones in terms of numerical stability are shown in Figs. 4, 5, and 6. Fig. 4 shows that explicit methods AB(2) and midpoint rule converge with only small time steps. To illustrate this point, Figs. 5 and 6 show the rotor angles of the three generators near the faulted bus provided by the TSCOPF solution using method AB(2). As the contingency is the same, the solution should be very similar. However, as the time step increases from 20 to 25 ms, the rotor angles of the two generators exhibit increasing oscillations. This is problematic because the solution in Fig. 6 can be considered valid if the results are not further inspected. It is noteworthy that these types of false solutions can be detected and removed by introducing additional constraints in the TSCOPF model. On the other hand, when the time step is sufficiently small, and AB(2) and the midpoint rule converge, they provide more conservative results than the other methods because their error constants are positive,as shown in Table 2.

Fig. 7 shows the CPU time required to converge to the solution. All the methods in this figure require more CPU time as the time step decreases because the number of equations and variables increases in the TSCOPF model. It can be observed that the trapezoidal rule provides the best performance in terms of CPU time. It can also be observed that MTR does not save much CPU time compared to the trapezoidal rule, despite reducing the number of equations and variables by 7.9 % and 9.25 %, respectively. ABM takes substantially longer on the CPU than the other methods because two extra equations are solved at each step. The SEABM and SIABM methods can save computation time compared with the ABM by using already computed values instead of predicting all variables. Therefore, SEABM and SIABM have fewer equations in their prediction stages than the ABM. However, the CPU times of SEABM and SIABM in TSCOPF studies are still much higher than that of AM(2), indicating that they are not yet appropriate substitutes for AM(2). It should be noted that all the two-step methods in Fig. 7 are initialized using the trapezoidal rule.

C. EFFECT OF THE INITIALIZATION METHOD ON TWO-STEPS METHODS

Different initialization methods can be used to determine the value of $\mathbf{x_1}$ in (20) in two-step algorithms. This section applies three different initialization methods – Euler's method, trapezoidal rule, and RK4 – to the most promising methods, according to the previous sections. Fig. 8 shows the increase in TSCOPF cost as a percentage of the OPF in each case.

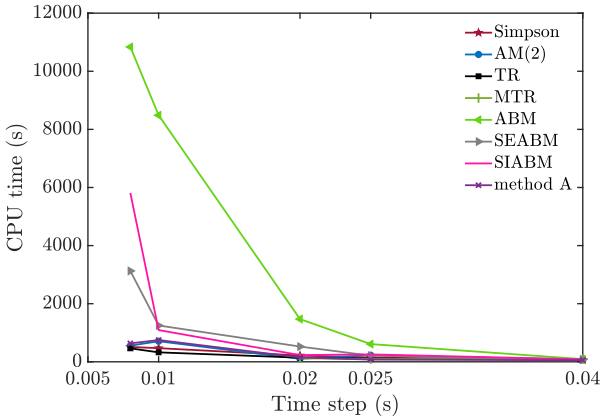

FIGURE 7. The CPU time for numerical methods to obtain the convergent solution. Fault 1.

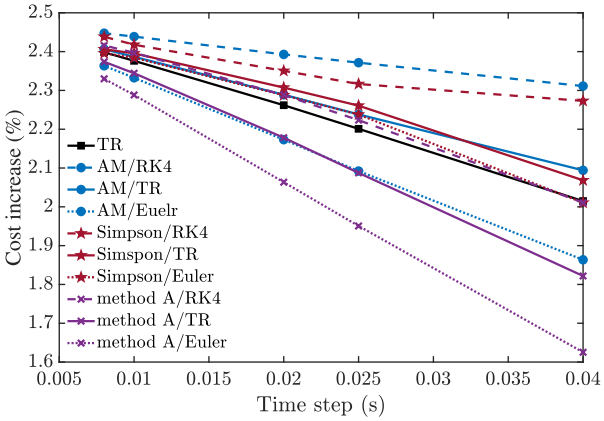

FIGURE 8. Increase in the TSCOPF generation cost compared to the OPF. Fault 1, using different initialization methods.

The RK4 initialization offers the most accurate results, whereas Euler initialization provides the least accurate results. With the RK4 initialization, the two-step methods AM(2), Simpson's rule and method A produce better results than the trapezoidal rule. The highest accuracy for time steps between 8 ms and 40 ms is given by AM(2), starting with RK4.

In addition to the sensitivity of the numerical methods to the time step, the total CPU time is another important factor to consider. Fig. 9 displays the CPU time vs. the absolute value of the convergence error for methods with different initializations. Each point in the figure corresponds to a different time step, from 8 ms to 25 ms. To calculate the absolute error, the generation cost of each method s is compared with the generation cost of a reference solution s_{ref}, obtained with AM(2), RK4 initialization and a time step of 8 ms:

$$\text{absolute error} = \left| \frac{s - s_{ref}}{s} \right| \times 100\% \tag{27}$$

The most efficient methods are those in the shaded area on the bottom left of Fig. 9, with a small error and a short CPU time. These methods are AM(2) with RK4 initialization and

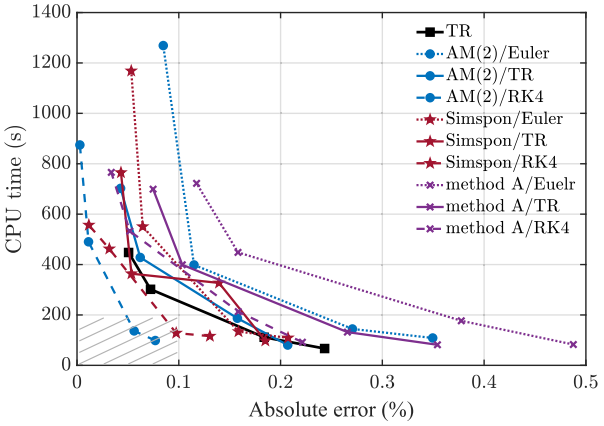

FIGURE 9. CPU time vs absolute value of the convergence error for different methods and time steps; Fault 1. The methods in the shaded area show the best performance.

TABLE 3. Contingencies.

Fault	Cost increase (%)	Total CPU time (s)	# Iterations
Fault 1	2.37	103.782	44
Fault 2	2.51	149.469	64
Fault 3	0	120.61	52
Fault 4	0	115	53
Fault 5	5.06	126.7	45
Fault 6	2.82	151.6	59

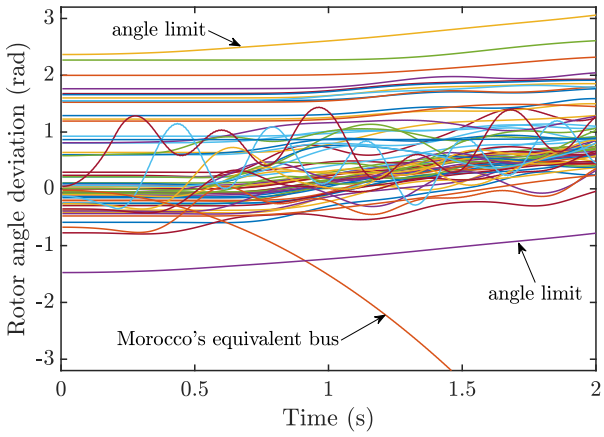

FIGURE 10. Synchronous generator rotor angles. Fault 3.

time steps of 25 and 20 ms, and Simpson's rule with RK4 initialization and a time step of 20 ms.

D. OTHER CONTINGENCIES

Similar results are obtained when different numerical methods are applied to other contingencies. Table 3 shows the increase in the TSCOPF total production cost, CPU time, and the number of iterations obtained by the Adams-Moulton method using the RK4 initialization and a time step of 25 ms.

Fault 2 is close to the easternmost tie-line between Spain and France. This fault results in a cost increment of 2.51 %, because part of the generation is re-dispatched to ensure that

TABLE 4. Summary of the investigated numerical methods.

Method	Accuracy	Computation time	Convergence
Adams-Bashforth, AB(2)	high	short	unstable
midpoint rule	low	short	unstable
Trapezoidal rule, TR	medium	short	stable
Simpson's rule	high	short	stable
Adams-Moulton, AM(2)	high	short	stable
BDF(2)	low	short	unstable
method A	low	short	stable
merged trapezoidal rule, MTR	medium	short	unstable
Adams-Bashforth-Moulton, ABM	medium	long	stable
semi-explicit Adams-Bashforth-Moulton, SEABM	high	long	stable
semi-implicit Adams-Bashforth-Moulton, SIABM	high	long	stable

the Iberian Peninsula system does not lose synchronism with the rest of continental Europe. As shown in Table 3, the solution to this fault requires significant computational effort in terms of the CPU time and iterations.

Fault 3 is close to the tie-line between Spain and Morocco. When the stability limit represented by (16) constrains the angle of the bus representing Morocco, there is no feasible solution. As a result, Morocco's aggregated bus is removed from (10) and (16), providing a solution in which the transient stability constraint is not violated, but the Moroccan system should be disconnected from the Iberian grid, as shown in Fig. 10. There is no cost increase due to Fault 3 in the case of the disconnection of Morocco.

Fault 4, regarded as a typical security issue in the Iberian Peninsula, does not violate the stability limits and, therefore, does not result in a re-dispatch of power production. Therefore, this fault is not a critical contingency in the studied scenario.

Faults 5 and 6 are the only studied incidents that are not short-circuits. Fault 5 is the loss of the largest operating power plant (2580 MW) in Portugal, leading to a 5.06 % cost increase owing to the resulting power imbalance. Fault 6 is the disconnection of the Iberian Peninsula from the rest of continental Europe, which increases the cost by 2.82 %.

Finally, the algorithms have been tested for different convergence starting points in voltages, angles, and active and reactive powers. The results are identical when different convergence starting points are applied to the same model, and the CPU time and the number of iterations are very similar.

VI. CONCLUSION

The main result of this study is that two of the studied methods outperform the trapezoidal rule, which has been, until now, the default method in TSCOPF models based on simultaneous discretization. These methods are Adams-Moulton of order two and Simpson's rule, both with RK4 in the initialization stage. The improvement they provide in terms of computing time and accuracy is best seen in Fig. 9.

The results also show that most methods converge and provide reasonably good results when a time step of 10 ms is used, which is typical in transient stability studies. However, the explicit methods fail to converge for time steps greater than 20 ms, and their application to the TSCOPF model can hide numerical instabilities. On the other hand, the implicit methods, except for the backward differentiation formula of order 2, converge for time steps as large as 50 ms. Consequently, the implicit methods with relatively large time steps can mitigate the computational burden of TSCOPF problems. Furthermore, it is shown that the newly formulated semi-explicit and semi-implicit predictor-corrector methods are not considerably more efficient than AM(2) in TSCOPF studies. Table 4 summarizes the performance of the numerical methods throughout the study and their main advantages and limitations. Finally, applying the TSCOPF model to the Iberian Peninsula system helped to identify faults that significantly impact the total generation cost. Three significant faults are found in the northeastern area of the analyzed system: one is a short-circuit near a large generator, the other is a short-circuit near a tie-line connection with France and the rest of continental Europe, and the third is a total disconnection of the Iberian Peninsula from the rest of continental Europe.

More studies on other real power systems could be useful to confirm these results, but there are no indications that the results will be different. In the future, new developments in mathematical integration methods must be evaluated for application in TSCOPF studies.

Conflict of Interest: The authors declare that they have no conflict of interest.

REFERENCES

[1] S. Xia, Z. Ding, M. Shahidehpour, K. W. Chan, S. Bu, and G. Li, "Transient stability-constrained optimal power flow calculation with extremely unstable conditions using energy sensitivity method," *IEEE Trans. Power Syst.*, vol. 36, no. 1, pp. 355–365, Jan. 2021.

[2] F. Arredondo, P. Ledesma, E. D. Castronuovo, and M. Aghahassani, "Stability improvement of a transmission grid with high share of renewable energy using TSCOPF and inertia emulation," *IEEE Trans. Power Syst.*, vol. 37, no. 4, pp. 3230–3237, Jul. 2020.

[3] S. Abhyankar, G. Geng, M. Anitescu, X. Wang, and V. Dinavahi, "Solution techniques for transient stability-constrained optimal power flow—Part I," *IET Gener., Transmiss. Distrib.*, vol. 11, no. 12, pp. 3177–3185, 2017.

[4] G. Geng, S. Abhyankar, X. Wang, and V. Dinavahi, "Solution techniques for transient stability-constrained optimal power flow—Part II," *IET Gener., Transmiss. Distrib.*, vol. 11, no. 12, pp. 3186–3193, Aug. 2017.

[5] M. Schlegel, K. Stockmann, T. Binder, and W. Marquardt, "Dynamic optimization using adaptive control vector parameterization," *Comput. Chem. Eng.*, vol. 29, no. 8, pp. 1731–1751, Jul. 2005.

[6] L. T. Biegler, A. M. Cervantes, and A. Wächter, "Advances in simultaneous strategies for dynamic process optimization," *Chem. Eng. Sci.*, vol. 57, no. 4, pp. 575–593, Feb. 2002.
[7] F. Arredondo, E. Castronuovo, P. Ledesma, and Z. Leonowicz, "Analysis of numerical methods to include dynamic constraints in an optimal power flow model," *Energies*, vol. 12, no. 5, p. 885, Mar. 2019.
[8] G. Geng, V. Ajjarapu, and Q. Jiang, "A hybrid dynamic optimization approach for stability constrained optimal power flow," *IEEE Trans. Power Syst.*, vol. 29, no. 5, pp. 2138–2149, Sep. 2014.
[9] Q. Jiang and Z. Huang, "An enhanced numerical discretization method for transient stability constrained optimal power flow," *IEEE Trans. Power Syst.*, vol. 25, no. 4, pp. 1790–1797, Nov. 2010.
[10] Q. Jiang and G. Geng, "A reduced-space interior point method for transient stability constrained optimal power flow," *IEEE Trans. Power Syst.*, vol. 25, no. 3, pp. 1232–1240, Aug. 2010.
[11] D. Gan, R. J. Thomas, and R. D. Zimmerman, "Stability-constrained optimal power flow," *IEEE Trans. Power Syst.*, vol. 15, no. 2, pp. 535–540, May 2000.
[12] A. Tiwari and V. Ajjarapu, "Optimal allocation of dynamic VAR support using mixed integer dynamic optimization," *IEEE Trans. Power Syst.*, vol. 26, no. 1, pp. 305–314, Feb. 2011.
[13] Y. Yuan, J. Kubokawa, and H. Sasaki, "A solution of optimal power flow with multicontingency transient stability constraints," *IEEE Trans. Power Syst.*, vol. 18, no. 3, pp. 1094–1102, Aug. 2003.
[14] H. W. Dommel and N. Sato, "Fast transient stability solutions," *IEEE Trans. Power App. Syst.*, vol. PAS-91, no. 4, pp. 1643–1650, Jul. 1972.
[15] J. R. Marti and J. Lin, "Suppression of numerical oscillations in the EMTP power systems," *IEEE Trans. Power Syst.*, vol. 4, no. 5, pp. 739–747, May 1989.
[16] J. Y. Astic, A. Bihain, and M. Jerosolimski, "The mixed Adams-BDF variable step size algorithm to simulate transient and long term phenomena in power systems," *IEEE Trans. Power Syst.*, vol. 9, no. 2, pp. 929–935, May 1994.
[17] J. Sanchez-Gasca, R. D'aquila, W. Price, and J. Paserba, "Variable time step, implicit integration for extended-term power system dynamic simulation," in *Proc. Power Ind. Comput. Appl. Conf.*, May 1995, pp. 183–189.
[18] T. Noda, K. Takenaka, and T. Inoue, "Numerical integration by the 2-stage diagonally implicit Runge–Kutta method for electromagnetic transient simulations," *IEEE Trans. Power Del.*, vol. 24, no. 1, pp. 390–399, Jan. 2009.
[19] D. Fabozzi and T. Van Cutsem, "Simplified time-domain simulation of detailed long-term dynamic models," in *Proc. IEEE Power Energy Soc. Gen. Meeting*, Jul. 2009, pp. 1–8.
[20] G. Tzounas, I. Dassios, and F. Milano, "Small-signal stability analysis of numerical integration methods," *IEEE Trans. Power Syst.*, early access, Jan. 27, 2022, doi: 10.1109/TPWRS.2022.3146345.
[21] A. Tutueva, T. Karimov, and D. Butusov, "Semi-implicit and semi-explicit Adams-Bashforth-Moulton methods," *Mathematics*, vol. 8, no. 5, p. 780, May 2020.
[22] A. Tutueva and D. Butusov, "Stability analysis and optimization of semi-explicit predictor–corrector methods," *Mathematics*, vol. 9, no. 19, p. 2463, Oct. 2021.
[23] F. Milano, "An open source power system analysis toolbox," *IEEE Trans. Power Syst.*, vol. 20, no. 3, pp. 1199–1206, Aug. 2005.
[24] R. Zarate-Minano, T. Van Cutsem, F. Milano, and A. J. Conejo, "Securing transient stability using time-domain simulations within an optimal power flow," *IEEE Trans. Power Syst.*, vol. 25, no. 1, pp. 243–253, Feb. 2010.
[25] M. Aghahassani, E. D. Castronuovo, P. Ledesma, and F. Arredondo, "Application of linear multi-step methods to a transient stability constrained optimal power flow model," in *Proc. IEEE Int. Conf. Environ. Electr. Eng. IEEE Ind. Commercial Power Syst. Eur. (EEEIC/I& CPS Europe)*, Jun. 2020, pp. 1–6.
[26] *Powerworld*. Accessed: Sep. 10, 2021. [Online]. Available: https://www.powerworld.com/
[27] M. Y. Borodulin, "Effect of numerical integration on critical time evaluation in power system stability studies," in *Proc. IEEE Power Energy Soc. Gen. Meeting*, Jul. 2013, pp. 1–5.
[28] K. Prabhashankar and W. Janischewsyj, "Digital simulation of multimachine power systems for stability studies," *IEEE Trans. Power App. Syst.*, vol. PAS-87, no. 1, pp. 73–80, Jan. 1968.
[29] K. Stanton and S. Talukdar, "New integration algorithms for transient stability studies," *IEEE Trans. Power App. Syst.*, vol. PAS-89, no. 5, pp. 985–991, May 1970.
[30] G. Wanner and E. Hairer, *Solving Ordinary Differential Equations II*. Berlin, Germany: Springer, 1996, vol. 375.
[31] D. F. Griffiths and D. J. Higham, *Numerical Methods for Ordinary Differential Equations: Initial Value Problems*. London, U.K.: Springer, 2010.
[32] F. E. Cellier and E. Kofman, *Continuous System Simulation*. New York, NY, USA: Springer, 2006.
[33] Q. Zhou and J. W. Bialek, "Approximate model of European interconnected system as a benchmark system to study effects of cross-border trades," *IEEE Trans. Power Syst.*, vol. 20, no. 2, pp. 782–788, May 2005.
[34] N. Hutcheon and J. W. Bialek, "Updated and validated power flow model of the main continental European transmission network," in *Proc. IEEE Grenoble Conf.*, Jun. 2013, pp. 1–5.
[35] *GAMS—Cutting Edge Modeling*. Accessed: Sep. 10, 2021. [Online]. Available: https://www.gams.com/
[36] A. Wächter and L. T. Biegler, "On the implementation of an interior-point filter line-search algorithm for large-scale nonlinear programming," *Math. Program.*, vol. 106, no. 1, pp. 25–57, May 2006.
[37] *IPOPT documentation*. Accessed: Sep. 10, 2021. [Online]. Available: https://coin-or.github.io/Ipopt/
[38] L. S. Vargas, V. H. Quintana, and A. Vannelli, "A tutorial description of an interior point method and its applications to security-constrained economic dispatch," *IEEE Trans. Power Syst.*, vol. 8, no. 3, pp. 1315–1324, Aug. 1993.

MOHAMMADAMIN AGHAHASSANI received the B.Sc. degree in electrical engineering from the Amirkabir University of Technology, Iran, in 2013, and the M.Sc. degree in electrical engineering from the Politecnico de Milano, Italy, in 2017. He is currently pursuing the Ph.D. degree with the Department of Electrical Engineering, Universidad Carlos III de Madrid, Spain. He has been an Academic Visitor at University College Dublin, Ireland. His research interests include power system optimization and transient stability analysis.

EDGARDO D. CASTRONUOVO (Senior Member, IEEE) received the B.S. degree in electrical engineering from the National University of La Plata, Argentina, in 1995, the M.Sc. and Ph.D. degrees from the Federal University of Santa Catarina, Brazil, in 1997 and 2001, respectively, and the Ph.D. degree from INESC TEC, Portugal, in 2005. He worked with the CEPEL, Brazil, and INESC TEC. He is currently a Professor with the Department of Electrical Engineering, University Carlos III of Madrid, Spain, on leave from CentraleSupèlec, France. His research interests include are in optimization methods applied to power system problems, renewable generation, and storage. He is the Vice-President of the IEEE Spain Section.

PABLO LEDESMA received the Ph.D. degree from the University Carlos III of Madrid, in 2001. He is currently an Associate Professor with the University Carlos III of Madrid. He has worked with the Spanish TSO on several projects in large-scale integration of renewable energy. He is an Academic Visitor with Chalmers University, Sweden, and Strathclyde University, U.K. His research interests include are transient stability and dynamic modeling of power systems.

FRANCISCO ARREDONDO received the Ph.D. degree in electrical engineering from the University Carlos III of Madrid, in 2019. He is currently an Assistant Professor with the University Carlos III of Madrid. He has been an Academic Visitor with the Wrocław University of Technology, Poland. His research interests include the power system stability, renewable generation, energy storage systems, and mathematical optimization methods.